

# Indentation size effect and Vickers microhardness measurement of metal-modified arsenic chalcogenide glasses

T. KAVETSKYY<sup>a,b</sup>, J. BORC<sup>c</sup>, K. SANGWAL<sup>c\*</sup>, V. TSMOTS<sup>a</sup>

<sup>a</sup>*Solid State Microelectronics Laboratory, Drohobych Ivan Franko State Pedagogical University, ul. I. Franko 24, Drohobych, 82100, Ukraine*

<sup>b</sup>*Institute of Materials, Scientific Research Company "Carat", ul. Stryjska 202, Lviv, 79031, Ukraine*

<sup>c</sup>*Department of Applied Physics, Lublin University of Technology, ul. Nadbystrzycka 38, 20-618 Lublin, Poland*

The experimental results of a systematic investigation of the microhardness of two systems of metal-modified arsenic chalcogenide glasses:  $X_x(\text{As}_2\text{S}_3)_{100-x}$  ( $x = 0$  or  $15$ , and  $X = \text{Ag}$  and  $\text{AgI}$ ) and  $\text{As}_2\text{Se}_3$  without and with  $0.5$  at.% RE (RE = Nd, Sm, Ho and Er) for applied indentation load ranging from  $0.005$  to  $1$  N are described and discussed. It was found that, with an increase in load  $P$ , for both systems the microhardness  $H_V$  first increases, then decreases showing a maximum hardness  $H_{\text{max}}$ , and finally increases again after attaining a minimum hardness  $H_{\text{min}}$ . Analysis of the experimental data on hardness  $H_V$  as a function of indentation diagonal  $d$  according to the relation:  $H = H_0(1+d_0/d)$ , where  $H_0$  is the load independent hardness and  $d_0$  is a constant, revealed that: (1) doping substances lead to the softening of  $\text{As}_2\text{S}_3$  samples and hardening of  $\text{As}_2\text{Se}_3$  samples, and the hardening of the matrix may be attributed to the size of doping substance, (2) formation of cracks in chalcogenide glasses follows the general concepts of fracture mechanics and their generation depends only on the basic glass matrix but is not affected by dopants and their chemical nature, and (3) the load-independent indentation microhardness  $H_0$  of a sample may be determined only from indentation data obtained in the load interval where  $H_V$  decreases with an increase in applied  $P$ .

(Received September 24, 2010; accepted October 14, 2010)

*Keywords:* Arsenic chalcogenide glasses, Dopants, Indentation cracks, Indentation hardness, Indentation size effect.

## 1. Introduction

Mechanical properties of materials play important role for their practical applications and are intimately connected with their structure and other physical and chemical properties. Among the various experimental techniques, indentation hardness testing is frequently used for the determination of mechanical properties of crystalline materials in the form of bulk samples and thin films. There is indeed voluminous literature dealing with the determination of indentation hardness of crystalline materials (for the literature see [1,2]). However, it is well known that the measured microhardness  $H$  of solids usually depends on the applied indentation test load  $P$ . This phenomenon is known as the indentation size effect (ISE). There are two types of ISE: (1) normal ISE and (2) reverse ISE. In the former case the measured hardness decreases with increasing test load, while in the latter case the measured hardness increases with an increase in the applied load. In contrast to the crystalline solids, until now indentation size effect has not been investigated for noncrystalline solids. Previous works in the area of indentation deformation of glasses deal with the nature of flow and fracture in the deformed zone [3-6].

Arsenic chalcogenide glasses are widely used in modern optoelectronics [7-9]. In search of new materials with improved properties high attention has been paid to

the doping of arsenic chalcogenide glasses by metal atoms. Depending on the doping element, amorphous arsenic chalcogenides become infrared amplifier (e.g. rare-earth doped As-Se glasses [10]), ionic conductors (e.g. Ag-As-S glasses [11]) or electrical conduction changes (e.g. from  $p$ - to  $n$ -type in Bi-Ge-Se glasses [12]). The effect of some dopants on the physical properties of arsenic chalcogenide systems has also been investigated [13,14]. Chalcogenide glasses are known to exhibit a variety of light-induced phenomena such as photoexpansion, photofluidity, photocrystallization and photoplasticity [15,16]. Consequently, it was thought worthwhile to carry out a systematic investigation of microindentation deformation of two systems of bulk metal-modified arsenic chalcogenide glasses:  $X_x(\text{As}_2\text{S}_3)_{100-x}$  ( $x = 0$  or  $15$ , and  $X = \text{Ag}$  and  $\text{AgI}$ ) and  $\text{As}_2\text{Se}_3$  without and with  $0.5$  at.% RE (RE = Nd, Sm, Ho and Er) in a wide range of applied indentation load. The aim of the study was three-fold: (1) to determine the load dependence of microhardness of the above noncrystalline samples and to establish some general trends for the load dependence of microhardness, (2) to analyze the experimental data on load dependence of hardness using the approaches advanced to explain ISE in crystalline solids, and (3) to understand the effect of dopants on the microhardness of the investigated noncrystalline solids.

## 2. Experimental

The bulk samples for indentation deformation were prepared by the conventional melt-quenching technique in evacuated quartz ampoules from appropriate mixtures of high purity precursors [14,17,18]. The amorphous state of the prepared samples was verified by x-ray diffraction analysis using the HZG-4a diffractometer (Cu  $K_{\alpha}$ -radiation). From the ingots bulk samples in the form of disks of about 1–1.5 mm thickness were cut and subsequently polished using diamond paste with grain size 0.8  $\mu\text{m}$  to yield high optical-quality surfaces for measurements. To remove mechanical strains developed during the synthesis, cutting and polishing procedure, the samples were annealed for 1 h at a temperature 20–30 K below the glass transition temperature.

Indentations were made on the samples using Anton Paar MHT-10 hardness tester fitted to a Carl Zeiss “Axiotech” metallurgical microscope and Polaroid camera. Loads  $P$  ranging from 0.005 to 1 N were used for indentation time of 10 s. The offset of diagonal tip was  $< 0.25 \mu\text{m}$  and the load resolution was 0.001 N. To avoid overlapping of surface stresses developed around neighbouring indentations the separation between indentation diagonals was kept more than ten times the diagonal length of indentation impressions. The dimensions of both diagonals  $d$  made at a particular load  $P$  were measured, and the average diagonal  $d$  was calculated. The value of microhardness  $H_V$  was computed from the  $P(d)$  data using the standard relation [19,20]:

$$H_V = kP/d^2, \quad (1)$$

where  $k$  is a geometrical conversion factor for the indenter used. The average values of indentation diagonal  $d$  and microhardness  $H_V$  for at least 5 indentations were used in the analysis of indentation size effect and hardness measurements. In the case of the Vickers indenter when  $P$  is taken in N and  $d$  in  $\mu\text{m}$ , the geometrical conversion factor  $k = 0.1891$  and hardness  $H_V$  is in VHN (1 VHN = 9.8 MPa). The standard deviation was about 10% from the average microhardness measured on a sample at the low loads whereas this deviation was 3–4% at high loads.

In order to obtain experimental data on the load dependence of radial cracks developed at the corners of indentations, the length  $c$  of radial cracks formed around indentations formed at a particular load  $P$  was measured manually using a filar micrometer eyepiece from the centre of indentations to the crack tip. An average value of crack length  $c$  was calculated from the measured values of all cracks around the indentations made at a particular load  $P$ . The standard deviation in the average crack length was found to be up to 15%.

## 3. Results

It was observed that well-defined indentations are produced on the surfaces of all samples at loads below a particular load  $P_c$  but for loads exceeding  $P_c$  radial cracks originating from one of the corners of indentations or in the vicinity of the corners develop around them. The above features may be noted from Figs. 1 and 2, which illustrate

examples of indentation imprints produced on  $\text{As}_2\text{S}_3$ -Ag/AgI and  $\text{As}_2\text{Se}_3$ :RE systems, respectively, at different loads.

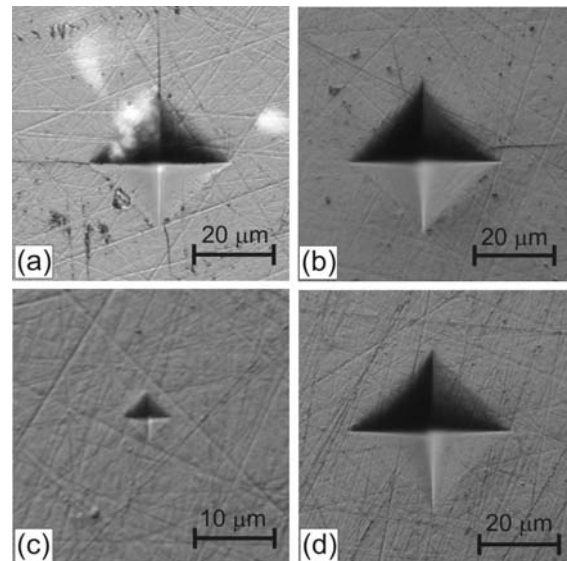


Fig. 1. Typical examples of indentations produced on (a)  $\text{As}_2\text{S}_3$ , (b)  $(\text{As}_2\text{S}_3)_{85}\text{Ag}_{15}$ , and (c,d)  $(\text{As}_2\text{S}_3)_{85}(\text{AgI})_{15}$  samples at different loads  $P$ : (a) 0.8 N, (b,d) 1 N and (c) 0.02 N.

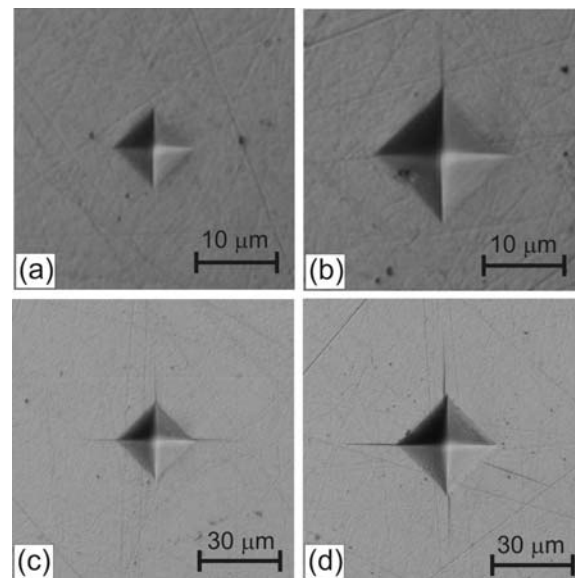


Fig. 2. Examples of indentations produced on  $\text{As}_2\text{Se}_3$ :Er sample at different loads: (a) 0.07 N, (b) 0.2 N, (c) 0.6 N and (d) 1 N.

The value of the load above which cracks are produced depend on the indented sample. Table 1 shows the values of  $P_c$  and the corresponding hardness  $H_V$  for different samples. Since the indentations were made at particular values of load  $P$ , it is difficult to establish the precise value of  $P_c$  when cracks are produced. Therefore, the values of  $P_c$  and  $H_V$  given in the table refer to the ranges of loads

and hardness when cracks are likely to be produced. It may be noted from Table 1 that The value of the load  $P_c$  is related to the microhardness  $H_V$  of a sample. The higher the microhardness  $H_V$  of a sample, the lower is the value of  $P_c$  for the sample.

Table 1. Values of  $P_c$  and corresponding  $H_V$  for different samples.

Sample	$P_c$ (N)	$H_V$ (VHN)
$As_2S_3$	0.6–0.8	135.3–139.1
$(As_2S_3)_{85}Ag_{15}$	0.6–0.8	130.5–134.2
$(As_2S_3)_{85}(AgI)_{15}$	0.8–1.0	114.6–120.4
$As_2Se_3$	0.6–0.8	137.7–135.6
$As_2Se_3:Nd$	0.2–0.4	148.2–144.7
$As_2Se_3:Sm$	0.2–0.4	148.3–143.4
$As_2Se_3:Ho$	0.1–0.2	150.1–147.8
$As_2Se_3:Er$	0.1–0.2	146.9–144.8

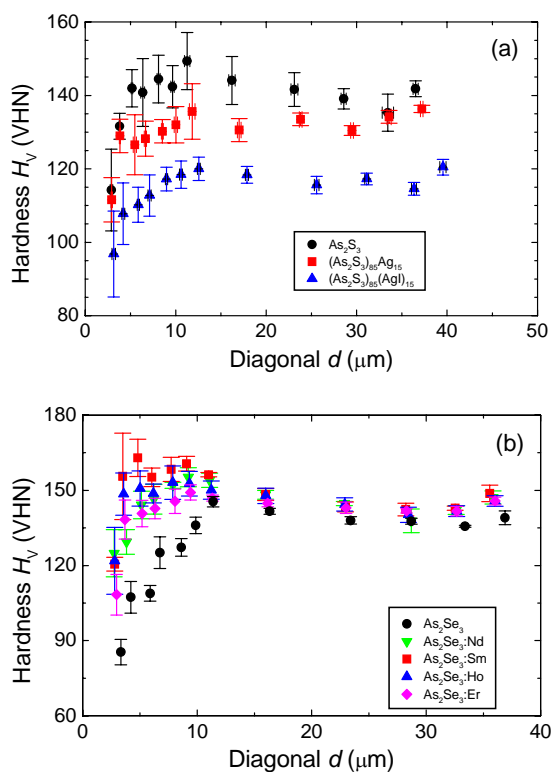


Fig. 3. Plots of  $H_V$  against indentation diagonal  $d$  for (a)  $As_2S_3$ -Ag/AgI and (b)  $As_2Se_3$ :RE systems. Note the appearance of reverse ISE in the interval of relatively low and high values of indentation diagonals  $d$  (i.e. in intervals I and III) and normal ISE in the interval of intermediate  $d$  (i.e. in interval II).

It was observed for both  $As_2S_3$ -Ag/AgI and  $As_2Se_3$ :RE (RE = Nd, Sm, Ho and Er) systems that, with an increase in load  $P$ , for both systems the microhardness  $H_V$  first increases, then decreases showing a maximum hardness

$H_{max}$ , and finally increases again after attaining a minimum hardness  $H_{min}$ . This means that, in the investigated range of applied load  $P$  one observes reverse ISE in the range of very low loads  $0.005 \text{ N} < P < 0.1 \text{ N}$ , then normal ISE in the range of intermediate loads  $0.1 \text{ N} < P < 0.8 \text{ N}$ , and finally reverse ISE again in the range of high loads  $0.005 \text{ N} < P < 0.1 \text{ N}$  and  $P > 0.6 \text{ N}$ . This behaviour of normal and reverse ISE is shown in Fig. 3a and b for  $As_2S_3$ -Ag/AgI and  $As_2Se_3$ :RE systems, respectively, in the form of plots of  $H_V$  as a function of indentation diagonal  $d$ . The dependence of  $H_V$  on  $P$  is not shown here to illustrate ISEs for the investigated glasses, because this dependence was similar to that of Fig. 3.

It should be mentioned that the microhardness  $H_V$  of 180 VHN for bulk arsenic-sulphide glass for an applied load of 0.5 N, reported by Sava [21], is comparable with the hardness values observed in the present study but the above types of three different and distinct load ranges of ISEs (i.e. an initial reverse ISE at low loads, followed by a normal ISE at intermediate loads, and finally a second reverse ISE at high loads) have not been observed in the case of noncrystalline (amorphous) as well as crystalline solids so far. However, there are indications that two distinct load regions of ISEs are indeed encountered in crystals [2].

## 4. Discussion

### 4.1. General considerations

Amorphous chalcogenides in the form of bulk and films show photoplastic effects [22,23]. For example, microindentation experiments made on as-deposited amorphous  $As_xSe_{100-x}$  thin films in the dark showed that the films are brittle but, upon exposure to illumination by a laser diode, they become soft and fluid as revealed by significant increase in indenter penetration depth and appearance of fluidity zones similar to those observed in metals [23]. However, after long-time exposure of the samples to laser light the indenter penetration depth attains a constant value [23], suggesting that long-time exposure of glasses to illumination does not influence microhardness measured at a particular applied load. Moreover, the larger photo-induced effects were observed for Se-rich materials like  $As_{10}Se_{90}$ ,  $As_{20}Se_{80}$  and but not for stoichiometric glass  $As_2Se_3$  i.e.  $As_{40}Se_{60}$  [18]. Thus, it can be argued that the above-bandgap photoexposure effects will be negligible for our conditions of hardness measurements on the  $As_2S_3$  and  $As_2Se_3$  based chalcogenide glasses.

It is well known that the indentation deformation behaviour of glasses is associated with the occurrence of intersecting flow lines due to shear displacements in the deformed zone under indentations [3,5] and depends on the composition of glasses [4] and their temperature [6]. Depending on their deformation behaviour, glasses are considered normal or anomalous. At room temperature, normal glasses are characterized by well-defined sharp indenter patterns [4,5], whereas anomalous glasses show complex indentation patterns [4,6]. However, glasses showing anomalous indentation patterns at low temperatures become "normal" with an increase in

temperature [6]. High silica content (> 80 wt%) is typical of anomalous glasses but normal glasses have relatively low silica content (< 80 wt%) and contains various oxide modifiers in different proportion.

In his classic work [3], Peter observed transformation from densification to plasticity in the deformation behaviour of glasses as the modifier content was increased. Later studies on indentation patterns showed [4,5] that normal glasses deform mainly by a shear flow process involving breaking and making of bonds between neighbours whereas anomalous glasses deform by a pressure-dominated densification process. It is believed [4] that deformation in anomalous glasses involves relative movement of atoms in a rigid covalent silica network but oxide modifiers facilitate deformation in normal glasses by providing easy slip paths through the silica network. In general, the composition dependence of physical properties of glasses is determined by the ratio of structural units and by the defect subsystem [24].

Examination of indentation imprints in Figs. 1 and 2 shows that our chalcogenide glass samples are essentially similar to those observed in normal glasses at low temperatures and anomalous glasses at high temperatures. The indentation imprints are well-defined and only radial cracks emanating from corners of indentations are produced.

#### 4.2. Shear-transformation-zone theory of amorphous plasticity

Atomic pictures of the structure of glass are constructed to interpret such observations as viscosity of supercooled liquids, inelastic scattering of light and plastic deformation. In the first picture, glass is considered to be composed of built-in cohesive nanometric domains containing several domains of approximately the same size inside which the vibrational motion of the domains are correlated [25]. This model has been used to explain inelastic x-ray scattering from glasses [25,26]. The second picture, used to explain deformation of amorphous solids, is essentially based on the concept that localized deformable clusters of molecules, called flow defects or shear transformation zones (STZs), enable noncrystalline solids to undergo irreversible shear strains in response to applied stresses [27-29]. These flow defects (i.e. domains, clusters or STZs) are small regions, consisting of 5 to 10 molecules in special configurations, undergo inelastic rearrangement in response to shear stresses [27]. In the case of binary arsenic chalcogenide glasses, the so-called closed cluster model has been advanced to explain their structural and electronic properties [8,30]. The model postulates the presence of cage-like, closed clusters without dangling bonds, composed of arsenic and chalcogen atoms in stoichiometric ratio, as plastic units of different dimensions packed randomly in space. In order to explain light-induced effects the concept of generation of valence alteration pairs involving point-like charged coordination defects has been advanced.

According to the shear transformation zone theory [27-29,31], in the presence of shear stress, STZs deform by a finite amount in one direction (elastic deformation) before becoming jammed and, when jammed in one direction, they transform in the opposite direction in response to a

reversed stress. Moreover, STZs are short-lived and are created and annihilated during irreversible (plastic) deformation. The STZ model also predicts “ductile to brittle” deformation as a function of strain rate and material failure at high strain rates [31]. These predictions are similar to the effect of decreasing temperature on the deformation of glasses mentioned above. According to the STZ theory, the curves of tensile stress as a function of strain at different temperatures and strain rates reveal a number of general features [28-29,31]. With increasing strain  $\varepsilon$ , the tensile stress  $\sigma$  at fixed strain rates first increases through a maximum at some value of strain, corresponding to yield stress, then begins to decrease and attains a steady state value, and finally material failure occurs due to shear heating and local disorder. The theory also predicts that the maximum at about the same strain  $\varepsilon$  in the stress-strain curves diminishes with an increase in temperature and a decrease in strain rate and is associated with the “ductility” of the material under study.

The nature of the theoretically predicted stress-strain curves are very similar to those of Vickers hardness  $H_V$  versus indentation diagonal size  $d$ , shown in Fig. 3a,b for different samples of chalcogenide glasses. Following Tabor [32], and Hammond and Armstrong [33], we define hardness stress  $\sigma_H$  as applied load  $P$  divided by projected contact area  $A = d^2/2$ , whereas indentation strain  $\varepsilon$  as the ratio of indentation diagonal  $d$  and indenter tip diameter  $D \approx 0.25 \mu\text{m}$ . Then one has  $H_V = k\sigma_H/2 = 0.0945\sigma_H$  (cf. Eq. (1)) and  $d = \varepsilon D$ . In the above analysis we have neglected elastic hardness strains accompanying Vickers hardness stresses because the elastic strain for the stress-strain curves for the glasses investigated here are negligibly small compared to the residual plastic strain [33] represented by the  $d$  values shown in Fig. 3.

#### 4.3. Nature of indentation size effect in chalcogenide glasses

Several approaches are known to describe the normal and reverse ISE behaviour of crystalline materials (see [1,2]). These approaches are based on the concept of generation and motion of dislocations beneath the indenter in the indented surface of a given single crystal. In fact, the generation and motion of dislocations is possible in the case of indentation of surfaces of ductile materials and semibrittle single crystals. Since in glasses it is difficult to imagine dislocation lines with displacement vectors (i.e. Burgers vectors) similar to those encountered in crystalline sides [34], the ISE observed on such materials cannot be attributed to occur by plastic deformation involving dislocations.

A popular relation between indentation load  $P$  and diagonal  $d$  is based on the separation of load-independent and load-dependent parts of the ISE of different types of materials, and is given in the form

$$P = ad + bd^2, \quad (2)$$

where the parameter  $a$  characterizes the load dependence of hardness and  $b$  is a load-independent constant. Following Li and Bradt [35,36], we shall refer to this as the proportional specimen resistance (PSR) model. The

term  $ad$  has been attributed to the specimen surface energy [37,38], the deformed surface layer [39], the proportional specimen resistance [35,36], the indenter edges acting as plastic hinges [40], and statistically stored dislocations [41,42]. We consider PSR model because it is not based on the concept of presence or generation of dislocations in a sample.

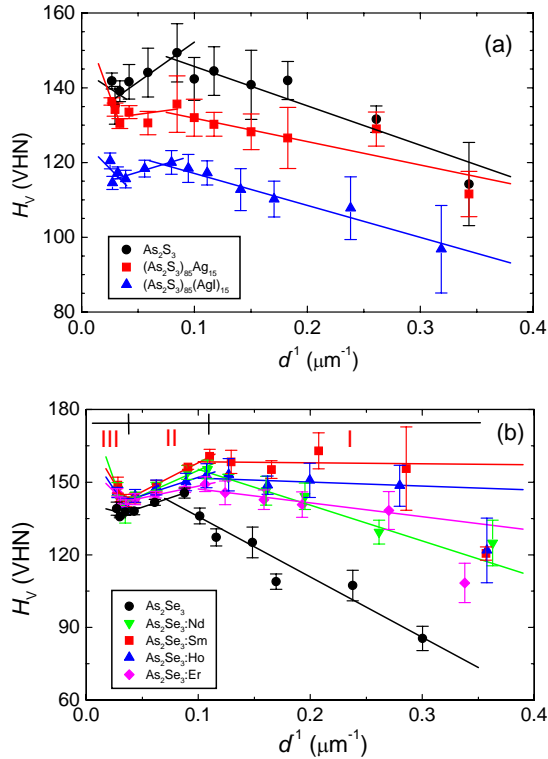


Fig. 4. Plots of  $H_V$  against  $d^{-1}$  for (a)  $As_2S_3$  and (b)  $As_2Se_3$  systems. Three intervals are indicated in (b). While analyzing the data of (b) in interval I points corresponding to the highest  $d^{-1}$  (i.e. the lowest  $d$ ) for the additives were omitted.

Multiplying Eq. (2) by  $k = 0.1891$  and taking  $P$  in  $N$  and  $d$  in  $\mu m$ , one may write

$$H = H_0(1 + d_0 / d), \quad (3)$$

where the load independent hardness  $H_0 = 0.1891b$  corresponds to the extrapolated hardness when  $d^{-1} = 0$  and the constant  $d_0 = a/b$ . The plots of  $H_V$  against  $d^{-1}$  for  $As_2S_3$  and  $As_2Se_3$  systems are shown in Fig. 4a and b, respectively. It is interesting to note that the experimental  $H_V(d^{-1})$  data for a given sample may be fitted according to relation (4) in three  $d^{-1}$  intervals, denoted by (I)  $d^{-1} > d_{max}^{-1}$ , (II)  $d_{max}^{-1} > d^{-1} > d_{min}^{-1}$  and (III)  $d^{-1} < d_{min}^{-1}$ , with different constants  $H_0$  and  $d_0$ . The values of the constants  $H_0$  and  $d_0$  in different  $d^{-1}$  intervals for various samples are listed in Table 2, while they are illustrated as histograms in Figs. 5 and 6 for  $As_2S_3$  and  $As_2Se_3$  systems, respectively.

The values of transition  $d_{max}^{-1}$  and  $d_{min}^{-1}$ , the corresponding hardness  $H_{max}$  and  $H_{min}$ , and the ratio  $d_0(I)/d_0(II)$  of the values of the constant  $d_0(I)$  and  $d_0(II)$  in intervals I and II are given in Table 3. The values of  $H_{max}$  and  $H_{min}$  and those of  $d_{max}^{-1}$  and  $d_{min}^{-1}$  of Table 3 were calculated using the calculated values of constants  $H_0$  and  $d_0$  listed in Table 1.

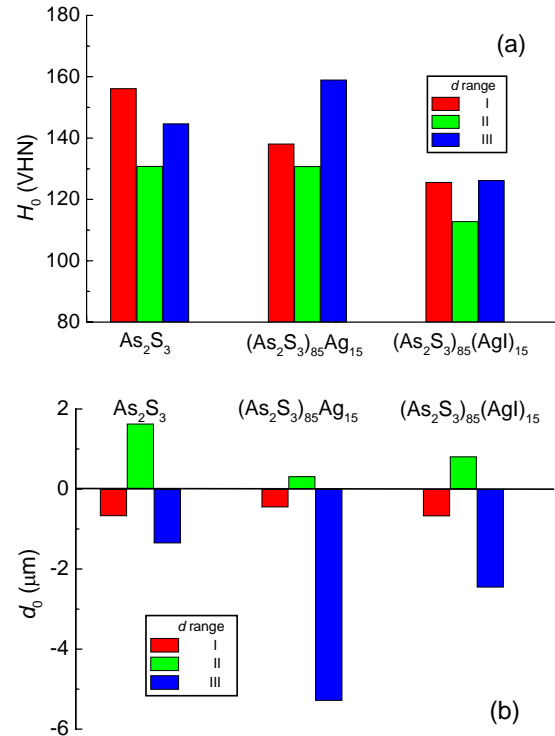


Fig. 5. Histograms of (a) load-independent microhardness  $H_0$  and (b) constant  $d_0$  in three intervals for different samples of  $As_2S_3$  system.

Description of the experimental  $H_V(d)$  data for different samples by Eq. (3) in terms of three well-defined intervals of indentation diagonals  $d$  with two transition diagonals  $d_{max}$  and  $d_{min}$  is interesting and may be attributed to stresses developed in the surface layer and in the volume of the indented samples. The values of thickness  $h$  of indentation surface layers where these transitions occur may be calculated from the relation:  $d = 7h$  for Vickers indenter [19,20]. Using the values of  $d_{max}^{-1}$  and  $d_{min}^{-1}$  given in Table 3 one finds that the initial deformed surface layer has thickness  $h_{max}$  of about  $2 \mu m$  for  $As_2S_3$ -Ag/AgI and pure  $As_2Se_3$  samples and about  $1.5 \mu m$  for  $As_2Se_3$ -RE samples. The initial increase in hardness with increasing indentation diagonal up to  $d_{max}$  is associated with the deformation of this surface layer (reverse ISE). The next surface layer extends up to  $h_{min} \approx 4 \mu m$ , where hardness decreases with increasing  $d$  (normal ISE). This means that the second layer is about  $2 \mu m$  thick for  $As_2S_3$ -Ag/AgI and pure  $As_2Se_3$  samples and about  $2.5 \mu m$  thick for  $As_2Se_3$ -RE samples. Obviously,

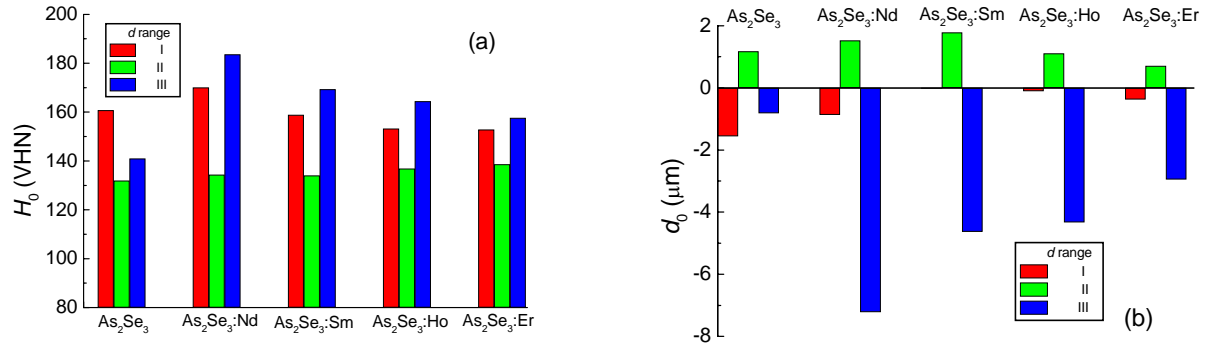


Fig. 6. Histograms of (a) load-independent microhardness  $H_0$  and (b) constant  $d_0$  in three intervals for different samples of  $As_2Se_3$  system.

Table 2. Values of  $H_0$  and  $d_0$  for different samples.

Sample	$d^{-1}$ interval	$H_0$ (VHN)	$d_0$ ( $\mu\text{m}$ )
$As_2Se_3$	$d^{-1} > d_{\max}^{-1}$	$156.23 \pm 3.43$	$-0.674 \pm 0.103$
	$d_{\max}^{-1} > d^{-1} > d_{\min}^{-1}$	$130.83 \pm 1.76$	$1.633 \pm 0.261$
	$d^{-1} < d_{\min}^{-1}$	$144.78 \pm 25.34$	$-1.356 \pm 5.42$
$(As_2S_3)_{85}Ag_{15}$	$d^{-1} > d_{\max}^{-1}$	$138.14 \pm 2.97$	$-0.454 \pm 0.107$
	$d_{\max}^{-1} > d^{-1} > d_{\min}^{-1}$	$130.78 \pm 2.88$	$0.319 \pm 0.417$
	$d^{-1} < d_{\min}^{-1}$	$159.03 \pm 1.26$	$-5.288 \pm 0.219$
$(As_2S_3)_{85}(AgI)_{15}$	$d^{-1} > d_{\max}^{-1}$	$125.62 \pm 1.34$	$-0.680 \pm 0.055$
	$d_{\max}^{-1} > d^{-1} > d_{\min}^{-1}$	$112.85 \pm 1.30$	$0.813 \pm 0.237$
	$d^{-1} < d_{\min}^{-1}$	$126.18 \pm 22.33$	$-2.455 \pm 5.786$
$As_2Se_3$	$d^{-1} > d_{\max}^{-1}$	$160.77 \pm 5.90$	$-1.553 \pm 0.203$
	$d_{\max}^{-1} > d^{-1} > d_{\min}^{-1}$	$131.92 \pm 0.70$	$1.174 \pm 0.088$
	$d^{-1} < d_{\min}^{-1}$	$140.97 \pm 13.01$	$-0.817 \pm 3.138$
$As_2Se_3:Nd$	$d^{-1} > d_{\max}^{-1}$	$170.10 \pm 2.77$	$-0.869 \pm 0.084$
	$d_{\max}^{-1} > d^{-1} > d_{\min}^{-1}$	$134.37 \pm 2.27$	$1.525 \pm 0.271$
	$d^{-1} < d_{\min}^{-1}$	$183.58 \pm 6.72$	$-7.212 \pm 0.908$
$As_2Se_3:Sm$	$d^{-1} > d_{\max}^{-1}$	$158.83 \pm 3.80$	$-0.026 \pm 0.134$
	$d_{\max}^{-1} > d^{-1} > d_{\min}^{-1}$	$134.08 \pm 0.96$	$1.784 \pm 0.116$
	$d^{-1} < d_{\min}^{-1}$	$169.30 \pm 17.57$	$-4.629 \pm 2.810$
$As_2Se_3:Ho$	$d^{-1} > d_{\max}^{-1}$	$153.23 \pm 1.90$	$-0.105 \pm 0.070$
	$d_{\max}^{-1} > d^{-1} > d_{\min}^{-1}$	$136.83 \pm 1.29$	$1.108 \pm 0.149$
	$d^{-1} < d_{\min}^{-1}$	$164.44 \pm 9.29$	$-4.3267 \pm 1.564$
$As_2Se_3:Er$	$d^{-1} > d_{\max}^{-1}$	$152.81 \pm 1.73$	$-0.372 \pm 0.063$
	$d_{\max}^{-1} > d^{-1} > d_{\min}^{-1}$	$138.60 \pm 0.249$	$0.706 \pm 0.028$
	$d^{-1} < d_{\min}^{-1}$	$157.61 \pm 11.98$	$-2.951 \pm 2.198$

Table 3. Values of transition  $d_{\max}^{-1}$  and  $d_{\min}^{-1}$  and corresponding hardness  $H_{\max}$  and  $H_{\min}$

Sample	$d_{\max}^{-1}$ ( $\mu\text{m}^{-1}$ )	$H_{\max}$ (VHN)	$d_{\min}^{-1}$ ( $\mu\text{m}^{-1}$ )	$H_{\min}$ (VHN)	$H_{\max}/H_{\min}$	$d_0(I)/d_0(II)$
$As_2Se_3$	0.075	148.3	0.035	138.3	1.072	0.413
$(As_2S_3)_{85}Ag_{15}$	0.075	133.4	0.035	132.2	1.009	1.693
$(As_2S_3)_{85}(AgI)_{15}$	0.075	119.3	0.035	116.1	1.028	0.836
$As_2Se_3$	0.071	143.0	0.035	137.1	1.043	1.323
$As_2Se_3:Nd$	0.095	156.1	0.035	141.5	1.103	0.570
$As_2Se_3:Sm$	0.095	158.4	0.035	142.5	1.112	0.015
$As_2Se_3:Ho$	0.095	150.7	0.035	142.1	1.061	0.095
$As_2Se_3:Er$	0.093	147.5	0.035	142.0	1.039	0.527

the second deformation layer has roughly the same thickness as the first layer in  $\text{As}_2\text{S}_3\text{-Ag/AgI}$  and pure  $\text{As}_2\text{Se}_3$  samples, but it is about 1.5 times thicker than the first layer in  $\text{As}_2\text{Se}_3\text{-RE}$  systems. Differences in the processes of deformation of these two layers are responsible for reverse and normal ISE in the samples. However, the increase in hardness for  $d > d_{\min}$  is mainly associated with the generation and development of radial cracks (reverse ISE).

Li and Bradt [35] pointed out that the quantities  $a$  and  $b$  of Eq. (3) are related to the elastic and plastic properties of a material, respectively. They also suggested that the quantity  $a$  consists of two contributions: (i) the elastic compression of the test specimen by the indenter, and (ii) the frictional resistance developed at the indenter facet/specimen interface. In the case of single crystals the former contribution is directly proportional to their Young's modulus  $E$ , while the latter is related to the indenter/specimen interface frictional effects. Following Li and Bradt [35], we assume that the  $a$  values are directly proportional to Young's modulus  $E$  of our amorphous solid samples alone and that the  $b$  values are a measure of their load-independent hardness  $H_0$  associated with the permanent deformation by indentation. Then the ratio  $E/H_0$  is a measure of the magnitude of the indentation residual stresses resulting from the mismatch between the plastic zone beneath the indentation and the surrounding elastic matrix. This means that, in the case of elastic compression alone (i.e. contribution (i) only), the ratio  $a/b$  may be considered as a measure of the residual stresses and is a constant quantity (i.e.  $a/b = \text{constant}$ ).

According to Li and Bradt [35], when elastic surface stresses are compressive the sign of  $a$  is positive. These compressive surface stresses result in normal ISE, as observed in interval (II) of Fig. 4. However, the negative values of  $a$  observed in intervals (I) and (III) suggest that the surface stresses are tensile, which implies that reverse ISE is associated with the relaxation of these surface stresses introduced in the deformation zone by indentation. Thus, it may be argued that relaxation of the surface stresses occurs as a result of competition between the deformation of near-surface layer and the bulk with increasing indenter penetration in the initial stage (I) at relatively low loads and development of indentation cracks in the sample bulk in interval (III) at high loads.

In glasses the anisotropic distribution of flow defects or shear transformation zones (STZs) and the associated anisotropic distribution of stresses in the plastically deformed zone may be attributed to the anisotropic creation and diffusion of flow defects by differences in the properties of the layers (cf. Sec. 4.2). At low indentation depths involving indenter penetration in the surface layer alone, it is possible that the generation and diffusion of flow defects is suppressed in the direction of indenter penetration by the underlying layer as a result of back stresses. This results in a flattened plastically deformed zone, as illustrated schematically in Fig. 7a. However, at high indentation depths when these back stresses are overcome, the generating flow defects are pushed faster by

the indenter in the direction of its penetration than those moving in the lateral direction. In this case, the plastically deformed zone is elongated in the direction of indenter penetration, as shown in Fig. 7b. At still higher indentation depths (i.e. at high applied stresses), both the rate of creation of flow defects and their concentration in the deformed zone increases rapidly, resulting in a situation when flow defects coalesce to develop into concentrated stresses [29,31], which ultimately lead to the generation of cracks.

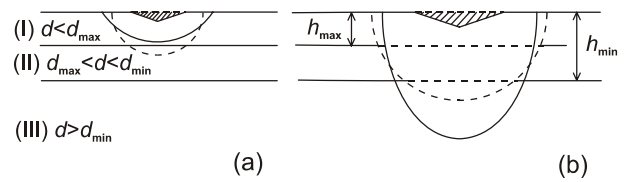


Fig. 7. Schematic presentation of cross-sectional profile of indentation impressions and accompanying hemispherical deformed zones in arsenic chalcogenide glasses at (a) small penetration and (b) intermediate penetration. Expected spherical and observed deformed zones are shown by dashed and solid lines, respectively. Different possible layers of thicknesses  $h_{\max}$  and  $h_{\min}$  corresponding to hardnesses  $H_{\max}$  and  $H_{\min}$  involved during indentation deformation from the indented surface are indicated.

#### 4.4. Microhardness of arsenic chalcogenide glasses and role of additives

It may be noted from Fig. 5a that the load-independent microhardness  $H_0$  essentially decreases in all the three  $d^{-1}$  intervals in the following sequence:  $\text{As}_2\text{S}_3$ ,  $(\text{As}_2\text{S}_3)_{85}\text{Ag}_{15}$  and  $(\text{As}_2\text{S}_3)_{85}(\text{AgI})_{15}$ , whereas in Fig. 6a, with an increase in the ionic radius  $r_a$  of rare earths,  $H_0$  of  $\text{As}_2\text{Se}_3\text{-RE}$  samples increases practically linearly in intervals I and III and decreases in interval II but the extrapolated value of the corresponding  $H_0$  at  $r_a = 0$  is different from that for the pure  $\text{As}_2\text{Se}_3$  sample. If one considers the magnitude of  $d_0$  alone in the three indentation depth intervals, it follows that the observed effect of an additive on  $H_0$  is essentially similar in the three intervals. Since the effect of an additive added to a matrix is to change its free energy  $F$ , the change in the free energy  $\Delta F$  of the matrix is expected to be related to mismatches in the size of the additive and host matrix. The simplest possible relation between  $\Delta F$  and additive radius  $r$  may be given by

$$\Delta F = A + B\Delta V/V_0 = A - B + B(r_a/r_0)^3 \approx A_1 + B_1 r_a, \quad (4)$$

where  $A$  and  $B$  are constants,  $\Delta V/V_0$  is the fractional volume misfit,  $r_a$  and  $r_0$  are the radii of additive species and host matrix, respectively,  $A_1 = (A - B)$ ,  $B_1 = B/3r_0$  and  $r_a/r_0 > 1$ . Identifying hardness  $H$  of samples with their free

energy  $F$ , one finds the expected dependence of  $H_0$  on the size  $r_a$  of the additive. However, the different extrapolated value of the corresponding  $H_0$  at  $r_a = 0$  from that for the pure  $\text{As}_2\text{S}_3$  sample implies that, apart from the size of an additive, other factors also determine the value of  $H_0$ .

The values of maximum and minimum hardness  $H_{\max}$  and  $H_{\min}$  show similar trends for the two systems. From these results it may be concluded that Ag and AgI lead to the softening of  $\text{As}_2\text{S}_3$  matrix but the softening effect of AgI is more than that of Ag on the  $\text{As}_2\text{S}_3$  matrix. This softening behaviour of  $\text{As}_2\text{S}_3$  matrix may be attributed to the size of doping substance. Calorimetric measurements on  $\text{GeS}_2\text{-Ag}_2\text{S}$  and  $\text{GeS}_2\text{-Ag}_2\text{S-AgI}$  glasses [43] as well as on AgI-doped tellurite oxide glasses [44] also lead to a similar conclusion. In contrast to the  $\text{As}_2\text{S}_3\text{-Ag/AgI}$  system, addition of rare earths to  $\text{As}_2\text{Se}_3$  matrix leads to its hardening. This effect of doping of rare earths can also be explained in terms of their size.

The anisotropy in hardness  $H_{\max}/H_{\min}$  for  $\text{As}_2\text{S}_3$  and  $\text{As}_2\text{Se}_3$  systems can equally be understood, as above, in terms of size of additive species. In this case the hardness anisotropy is directly connected with the ratio  $d_{0I}/d_{0II}$ , where  $d_{0I}$  and  $d_{0II}$  denote the values of  $d_0$  in intervals I and II, respectively. As mentioned in Sec. 4.1, since  $d_0 = a/b$  according to the PSR model, this means that the values of  $H_{\max}$  and  $H_{\min}$  are mainly determined by the relative contributions of  $a$  of neighbouring intervals.

In contrast to the trends of  $H_0$ , in Fig. 5b addition of Ag and AgI additives to  $\text{As}_2\text{S}_3$  matrix leads to a decrease in the value of constant  $|d_0|$  in intervals I and II but an increase in its value in interval III. As seen from Fig. 6b addition of rare earths to  $\text{As}_2\text{S}_3$  matrix leads to an increase in the value of  $|d_0|$  in interval III, but no well-relationship between  $|d_0|$  and the size of rare earths can be ascertained in intervals I and II. These trends reveal that there is poor relationship between  $H_0$  and  $d_0$  in the three intervals for both systems. This discrepancy in the trends of  $H_0$  and  $d_0$  may be attributed to the values of relaxation/contraction parameter  $d_0$ .

From the above discussion it may be concluded that the real load-independent indentation microhardness of a sample may be determined only from indentation data obtained in interval II, where one observes normal ISE. In fact, PSR model explains this ISE, and the extrapolated load-independent hardness  $H_0$  corresponding to  $d^{-1} = 0$  refers to this case (see Eq. (3)). These values of  $H_0$  are slightly lower than  $H_{\min}$  for a sample and the difference between  $H_0$  and  $H_{\min}$  is less than 6% (see Tables 2 and 3).

#### 4.5. Formation of indentation cracks

It may be noted from Table 1 that the value of the load  $P_c$  for the formation of cracks depends on the nature of dopant in a chalcogenide. In the case of  $\text{As}_2\text{S}_3$  system, Ag dopant does not lead to a change in  $P_c$  but AgI dopant increases the value of  $P_c$ . However, in  $\text{As}_2\text{S}_3$  system, all rare-earths lead to a marked decrease in  $P_c$ , but Ho and Er have more effect than Nd and Sm. This means that AgI dopant makes the generation of cracks difficult in  $\text{As}_2\text{S}_3$

system, but rare-earth dopants facilitate their generation in  $\text{As}_2\text{Se}_3$  system.

Generation of cracks of various types is a common observation on indented surfaces of glasses. As in the case of normal glasses, radial cracks are usually observed on the surfaces of bulk chalcogenide glasses (see Figs. 1 and 2). The formation of these indentation cracks is responsible for reverse ISE in stage III, and may be described by the general concepts of fracture mechanics.

According to fracture mechanics the length  $c$  of well-developed radial cracks extending from the centre of indentation is related to the applied load  $P$  by [45]

$$P/c^{2/3} = \beta_0 K_c + \beta_0 \sigma_s c^{1/2}, \quad (5)$$

where  $K_c$  is the fracture toughness for cracks,  $\sigma_s$  is the surface stress (i.e. residual stress confined to the surface layer after indentation) and  $\beta_0$  is a geometrical factor equal to 7 for Vickers indenter. The surface stresses  $\sigma_s$  can be tensile as well as compressive, and depending on whether they are tensile (i.e.  $\sigma_s > 0$ ) or compressive (i.e.  $\sigma_s < 0$ ), the surface traces of cracks expand or contract. Fig. 8 shows the dependence of  $P/c^{3/2}$  on  $c^{1/2}$  according to Eq. (5) for radial cracks observed on different undoped and doped  $\text{As}_2\text{Se}_3$  and  $\text{As}_2\text{S}_3$  samples.

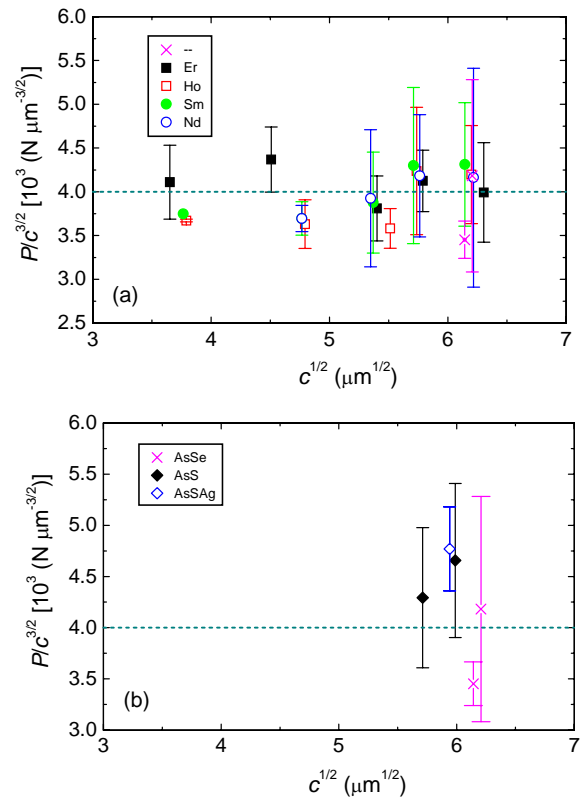


Fig. 8. Dependence of  $P/c^{3/2}$  on  $c^{1/2}$  for (a)  $\text{As}_2\text{Se}_3$  and (b)  $\text{As}_2\text{S}_3$  samples according to Eq. (5). Horizontal dashed curves in (a) and (b) present average value for  $\text{As}_2\text{Se}_3$  samples.

From Fig. 8 the following features may be noted:

- (1) The surface stress  $\sigma_s \approx 0$ , implies that the surface layer of the samples is in an equilibrium state at the time of measurements of crack length  $c$  after indentation.
- (2) Dopants do not change the fracture toughness  $K_c$  of  $\text{As}_2\text{Se}_3$  and  $\text{As}_2\text{S}_3$  glasses. This suggests that the dopants do not change the basic chalcogenide glass structure.
- (3) The fracture toughness  $K_c$  of  $\text{As}_2\text{Se}_3$  and  $\text{As}_2\text{S}_3$  glasses is about 0.57 and 0.64  $\text{MPa}\cdot\text{m}^{1/2}$ , respectively. These values of  $K_c$  are somewhat lower than those for silica glasses [4,6], but among the two chalcogenide glasses studied here,  $\text{As}_2\text{Se}_3$  glasses have a lower  $K_c$  than that of  $\text{As}_2\text{S}_3$  glasses.

From the above discussion it may be concluded that the formation of indentation cracks in arsenic-chalcogenide glasses involves two distinct processes: generation of cracks at indentation load  $P_c$  and their growth at  $P > P_c$ . The former process strongly depends on the presence of dopants in glass matrix and their chemical nature (see Table 1), whereas the latter process is essentially governed by fracture mechanics where fracture toughness  $K_c$  of a matrix does not depend on the glass matrix (see Fig. 8). Since creation and annihilation of flow defects under an indentation determines indentation deformation i.e. indentation size (see Sec. 4.2), the presence of dopants and their chemical nature are expected to affect the microhardness of arsenic chalcogenide glasses. In contrast to this, growth of cracks depends only on the basic glass matrix and is not affected by dopants and their chemical nature, because the process probably involves the dissipation of heat [31].

## 5. Summary and conclusions

From the load dependence of indentation deformation of two systems of metal-modified arsenic chalcogenide glasses:  $X_x(\text{As}_2\text{S}_3)_{100-x}$  ( $x = 0$  or 15, and  $X = \text{Ag}$  and  $\text{AgI}$ ),  $\text{As}_2\text{Se}_3$  and  $\text{As}_2\text{Se}_3 + 0.5$  at.% RE (RE = Nd, Sm, Ho and Er), the following conclusions may be drawn:

- (1) With an increase in applied load, Vickers microhardness  $H_V$  of arsenic chalcogenide glasses initially increases to a maximum value  $H_{\max}$ , then decreases to a minimum value  $H_{\min}$  and finally increases again until intense crack formation around indentations obliterate their square shape. The proportional specimen resistance (PSR) model of Li and Bradt [35,36], rewritten in the form of Eq. (4), satisfactorily describes the  $H_V(d)$  data in the three intervals of load  $P$  or indentation diagonal  $d$  and enables to calculate the values of the load-independent hardness  $H_0$  and constant  $d_0$  in different intervals for various samples.
- (2) Following the concepts of PSR model, with increasing indentation diagonal  $d$  the initial increase in microhardness of metal-modified arsenic chalcogenide glasses up to  $H_{\max}$  at small  $d$  and final increase in microhardness after  $H_{\min}$  for large  $d$  may be attributed to tensile surface stresses, while decrease in microhardness between  $H_{\max}$  and  $H_{\min}$  at intermediate indentation diagonal  $d$  to compressive elastic surface stresses. The tensile surface stresses at small and very large indentation diagonals  $d$  correspond to  $a < 0$ , while compressive surface stresses at intermediate indentation diagonal  $d$  corresponds to  $a > 0$ . Release of these surface stresses occurs due to elastic recovery in the near-surface layer up to  $d_{\max}$  when  $H_{\max}$  is attained and development of indentation cracks in the sample bulk after  $d_{\min}$  when  $H_{\min}$  is attained.
- (3) The initial reverse ISE followed by normal ISE in the investigated metal-modified arsenic chalcogenide glasses may be attributed to the flattening and elongation of hemispherical deformation zone in terms of differences in the mechanism of creation and diffusion of hole-like defects at low and high indentation depths, respectively, in the direction of indenter penetration.
- (4) The values of maximum and minimum hardness  $H_{\max}$  and  $H_{\min}$  show similar trends for the two systems. Doping substances lead to the softening of  $\text{As}_2\text{S}_3$  matrix and the hardening of  $\text{As}_2\text{Se}_3$  matrix. The softening and the hardening behaviour of the arsenic chalcogenide matrixes may be attributed *inter alia* to the size of doping substance.
- (5) Formation of indentation cracks in arsenic-chalcogenide glasses involves two distinct processes: generation of cracks at indentation load  $P_c$  and their growth at  $P > P_c$ . The former process strongly depends on the presence of dopants in glass matrix and their chemical nature, whereas the latter process is essentially governed by fracture mechanics where fracture toughness  $K_c$  of a matrix does not depend on the glass matrix. The difference in the effect of dopants on generation and growth of cracks is associated with the deformation process. The former involves generation and annihilation of flow defects whereas the latter probably involves the dissipation of heat.
- (6) The load-independent indentation microhardness  $H_0$  of a sample may be determined only from indentation data obtained in the interval of indentation diagonal  $d$  where  $H_V$  decreases with an increase in indentation size  $d$  (i.e. in the range of normal ISE). These values of  $H_0$  are slightly lower than  $H_{\min}$  for a sample and the difference between  $H_0$  and  $H_{\min}$  is less than 6%.

## Acknowledgments

This work was partly supported by the Ministry of Education and Science of Ukraine. The authors are indebted to Prof. Plamen Petkov, Prof. Tamara Petkova and Prof. Mihail Iovu for providing us with the samples of some arsenic chalcogenide glasses used for measurements. One of the authors (TK) also expresses his gratitude to Prof. Jacek Filipecki for his interest in this work and to International Visegrad Fund for a scholarship.

## References

- [1] K. Sangwal, Mater. Chem. Phys. **63**, 145 (2000).
- [2] K. Sangwal, Cryst. Res. Technol. **44**, 1019 (2009).
- [3] K.W. Peter, J. Non-Cryst. Solids **5**, 103 (1970).

- [4] A. Arora, D. B. Marshall, B. R. Lawn, M. V. Swan, *J. Non-Cryst. Solids* **31**, 415 (1979).
- [5] J. T. Hagan, *J. Mater. Sci.* **15**, 1417 (1980).
- [6] M. D. Michel, F. C. Serbena, C. M. Lipenski, *J. Non-Cryst. Solids* **352**, 3550 (2006).
- [7] D. Lezal, *J. Optoelectron. Adv. Mater.* **5**(1), 23 (2003).
- [8] M. Popescu, *J. Optoelectron. Adv. Mater.* **6**, 1117 (2004).
- [9] B. Bureau, X. H. Zhang, F. Smektala, J. -L. Adam, J. Troles, H. -Li Ma, C. Boussard-Pledel, J. Lucas, P. Lucas, D. Le Coq, M. R. Riley, J. H. Simmons, *J. Non-Cryst. Solids* **345-346**, 276 (2003).
- [10] D. Lezal, J. Pedlikova, J. Zavadil, P. Kostka, M. Poulain, *J. Non-Cryst. Solids* **326-327**, 47 (2003).
- [11] M. F. Kotkata, C. S. Mohamed, *J. Mater. Sci.* **24**, 1291 (1989).
- [12] N. Tohge, T. Minami, Y. Yamamoto, M. Tanaka, *J. Appl. Phys.* **51**, 1048 (1980).
- [13] F. Kyriazis, A. Chrissanthopoulos, V. Dracopoulos, M. Krbal, T. Wagner, M. Frumar, S. N. Yannopoulos, *J. Non-Cryst. Solids* **355**, 2010 (2009).
- [14] M. Iovu, S. Shutov, M. Popescu, D. Furniss, L. Kukkonen, A. B. Seddon, *J. Optoelectron. Adv. Mater.* **1**, 15 (1999).
- [15] M. L. Trunov, *J. Phys. D: Appl. Physics* **41**, 074011 (2008).
- [16] S. N. Yannopoulos, M. L. Trunov, *Phys. Stat. Solidi B* **246**, 1773 (2009).
- [17] K. Kolev, C. Popov, T. Petkova, P. Petkov, I. N. Mihailescu, J. P. Reithmaier, *Sensors and Actuators B: Chemical* **143**, 395 (2009).
- [18] R. Ya. Golovchak, A. Kozdras, O. Shpotyuk, *Solid State Comm.* **145**, 423 (2008).
- [19] B. W. Mott, *Microindentation Hardness Testing*, Butterworth, London (1956).
- [20] H. Bückle, in: J. H. Westbrook and H. Conrad (Eds.), *The Science of Hardness Testing and Its Research Applications*, ASME, Metal Park, OH (1973), p. 199.
- [21] F. Sava, *J. Optoelectron. Adv. Mater.* **3**, 425 (2001).
- [22] M. L. Trunov, *J. Optoelectron. Adv. Mater.* **7**, 2235 (2005).
- [23] M. L. Trunov, *J. Optoelectron. Adv. Mater.* **7**, 1223 (2005).
- [24] A. Feltz, *Amorphous Inorganic Materials and Glasses*, VCH, Weinheim (1993).
- [25] A. Mermet, E. Duval, A. Polian, M. Krisch, *Phys. Rev. E* **66**, 031510 (2002).
- [26] A. Mermet, A. Cunsolo, E. Duval, M. Krisch, C. Masciovecchio, S. Perghem, G. Ruocco, F. Sette, R. Verbeni, G. Viliani, *Phys. Rev. Lett.* **80**, 4205 (1998).
- [27] M. L. Falk, J. S. Langer, *Phys. Rev. E* **57**, 7192 (1998).
- [28] M. L. Falk, J. S. Langer, L. Pechenik, *Phys. Rev. E* **70**, 011507 (2004).
- [29] J. S. Langer, *Phys. Rev. E* **77**, 021502 (2008).
- [30] S. N. Yannopoulos, *Phys. Rev. B* **68**, 064206 (2003).
- [31] M. L. Manning, E. G. Daub, J. S. Langer, J. M. Carlson, *Phys. Rev. E* **79**, 016110 (2009).
- [32] D. Tabor, *The Hardness of Metals*, Clarendon Press, Oxford (1951).
- [33] B. L. Hammond, R. W. Armstrong, *Philos. Mag. Lett.* **57**, 41 (1988).
- [34] J. J. Gilman, *Chemistry and Physics of Mechanical Hardness*, Wiley, Hoboken NY (2009), Chap. 14.
- [35] H. Li, R. C. Bradt, *J. Mater. Sci.* **28**, 917 (1993).
- [36] H. Li, Y. H. Han, R. C. Bradt, *J. Mater. Sci.* **29**, 5641 (1994).
- [37] F. Fröhlich, P. Grau, W. Grellmann, *Phys. Stat. Sol. (a)* **42**, 79 (1977).
- [38] B. -D. Michels, G. H. Frischat, *J. Mater. Sci.* **17**, 329 (1982).
- [39] W. C. Oliver, R. Hutchings, J. B. Pethica, in: *Microindentation Techniques in Materials Science and Engineering*, P.J. Blau and B.R. Lawn (Eds.), ASTM, Philadelphia PA (1986), p. 90.
- [40] Q. Ma, D. R. Clarke, *J. Mater. Res.* **10**, 853 (1995).
- [41] W. D. Nix, H. Gao, *J. Mech. Phys. Solids* **46**, 411 (1998).
- [42] H. Gao, Y. Huang, W. D. Nix, J. W. Hutchinson, *J. Mech. Phys. Solids* **47**, 1239 (1999).
- [43] E. Robinel, B. Carette, M. Ribes, *J. Non-Cryst. Solids* **57**, 49 (1983).
- [44] C. Y. Zahra, A. -M. Zahra, *J. Non-Cryst. Solids* **190**, 251 (1995).
- [45] D. B. Marshall, B. R. Lawn, in: *Microindentation Techniques in Materials Science and Engineering*, P. J. Blau and B. R. Lawn (Eds.), (ASTM, Philadelphia PA (1986), p. 26.

\*Corresponding author: k.sangwal@pollub.pl